



CrossMark
click for updates

Cite this: *RSC Adv.*, 2015, 5, 97568

Molecular structures of Pr@C₇₂ and Pr@C₇₂(C₆H₃Cl₂): a combined experimental–theoretical investigation†

Yan-li Zhao,^{ab} Qin Zhou,^a Yong-fu Lian^{*a} and Hai-tao Yu^{*a}

A novel Pr-based monometallofullerene derivative, Pr@C₇₂(C₆H₃Cl₂), was successfully prepared and isolated. Its molecular composition was determined by matrix-assisted laser desorption ionization time-of-flight mass spectrometry. The molecular structure of Pr@C₇₂(C₆H₃Cl₂) was verified as Pr@C₂(10612)-C₇₂(C₆H₃Cl₂) by combined UV-visible-near-infrared absorption spectroscopy and quantum mechanics characterization, as well as a comparison with the structurally characterized analogue La@C₇₂(C₆H₃Cl₂). Furthermore, an additional computation indicated that the nonderivatized Pr@C₇₂ has the lowest-lying structure of Pr@C₂(10612)-C₇₂, followed by Pr@C_{2v}(11188)-C₇₂, which lies only 0.62 kcal mol⁻¹ above Pr@C₂(10612)-C₇₂. In addition, the temperature dependence of their thermodynamic distribution was estimated. We also analyzed the charge transfer and orbital interaction between the endohedral Pr atom and the carbon cage as well as the electronic configuration and formal charge state of the encapsulated Pr atom based on the computed quantum mechanics data.

Received 31st August 2015
Accepted 4th November 2015

DOI: 10.1039/c5ra17608e

www.rsc.org/advances

1 Introduction

Endohedral metallofullerenes (EMFs) have attracted a great deal of attention because of their unique structures and interesting properties relative to empty-cage fullerenes.^{1–4} Many significant applications of EMFs in such fields as materials science, nanoelectronics, and biomedicine have been proposed.^{5,6} The encapsulated metal atom(s) or metallic cluster can not only improve the performances of fullerenes to some extent but also result in new properties.^{7,8} Furthermore, the encapsulation extensively and profoundly aids our understanding of the nature of fullerenes.^{9–11}

Experimentally available EMFs have been well reviewed.^{5,12,13} Furthermore, many theoretical investigations have also been performed and summarized,^{14–16} which confirmed that the quantum mechanics computation is a very effective and indispensable method in combining the characterization of isomeric structures and stabilities with experiments.¹⁷

In early works, conventional EMFs were considered as those containing only one or two metal atoms.¹ Recently, several EMFs with three encapsulated metal atoms have been synthesized, for example, Er₃C₇₄,¹⁸ Dy₃C₉₈,¹⁹ and M₃C₈₀ (M = Tb,²⁰ Y,²¹ Sm²²). These findings greatly broaden the range of conventional

EMFs, although their structural isomers remain unclear, except for Sm₃C₈₀, the only trimetallofullerene whose structure has been unambiguously confirmed by single-crystal X-ray diffraction (XRD).²² As the simplest model systems, monometallofullerenes (mono-EMFs) are appropriate for understanding the nature of the interaction between the metal atom and the carbon cage. According to the formal charge of the encapsulated metal atom, the common mono-EMFs can be classified into two categories, divalent mono-EMFs and trivalent mono-EMFs. For the former, the encapsulated metals include alkali-earth atoms (Ca, Sr, Ba) and lanthanide atoms (Sm, Eu, Tm, and Yb),^{23,24} while for the latter, the encapsulated metals include Sc, Y, and lanthanide atoms, except for Sm, Eu, Tm, and Yb.^{25–27}

To date, the experimentally available empty fullerene molecules of a medium size (C_{2n}, 60 ≤ 2n ≤ 80) include C₆₀,²⁸ C₇₀,²⁹ C₇₆,³⁰ C₇₈,³⁰ and C₈₀.^{31,32} Interestingly, the C₇₂, C₇₄, and C₈₀ molecules were called “missing fullerenes”,³³ which are difficult to synthesize or isolate because of their structural instabilities or high chemical reactivity. The fullerene C₈₀ has been successfully isolated and structurally characterized.^{31,32} Theoretically, the C_{2v}(11188)-C₇₂ cage, which violates the well-known isolated pentagon rule (IPR),³⁴ *i.e.*, a non-IPR structure, was predicted to be the lowest-lying isomer among all of the possible C₇₂ structures, followed by the IPR isomer D_{6d}(11190)-C₇₂.³⁵ Generally, for the carbon cages with 2n > 72, the most thermodynamically stable isomer was believed to possess an IPR-satisfying structure. However, C₇₂ has been indisputably confirmed as the only example of the most stable isomer that possesses a non-IPR structure.³⁶ A theoretical analysis indicated that for the IPR isomer D_{6d}(11190)-C₇₂, the relatively large steric

^aKey Laboratory of Functional Inorganic Material Chemistry (Ministry of Education of China) and School of Chemistry and Materials Science, Heilongjiang University, Harbin 150080, PR China. E-mail: chyflian@hlju.edu.cn; yuhaitao@hlju.edu.cn

^bSchool of Pharmacy, Jiamusi University, Jiamusi 154007, PR China

† Electronic supplementary information (ESI) available. See DOI: 10.1039/c5ra17608e

repulsion originating from two peculiar hexagons surrounded by six hexagons should be responsible for its lower thermodynamic stability compared with the non-IPR cage $C_{2v}(11188)-C_{72}$.³⁷ Currently, no experimental evidence for the observation of $D_{6d}(11190)-C_{72}$ has been published. Although the isolation of the pure fullerene C_{72} is difficult, its chemical functionalization and encapsulation of metal(s) or a cluster are readily available.^{10,33,36,38–43}

Experimental reports have shown that several divalent metal atoms (for example, Ca,³³ Sr,³⁸ Eu,^{38,43} Tm,⁴⁴ and Yb³⁸) and trivalent metal atoms (for example, Er,⁴⁵ Lu,⁴⁴ Gd,⁴⁴ Y,³⁹ and La¹⁰) can be readily encapsulated into the C_{72} cage. For the fullerene C_{72} encapsulating a trivalent metal atom, the molecules $M@C_{72}$ ($M = \text{Er, Lu, Gd}$) are limited to mass spectrometry data,^{44,45} while the Y-EMF derivative, $Y@C_{72}(\text{CF}_3)$, has been isolated, and its UV-visible-near-infrared (UV-vis-NIR) absorption spectrum is available.³⁹ To date, the only structurally determined mono-EMF with a trivalent metal atom in the C_{72} cage is the mono-adduct $\text{La}@C_{72}(\text{C}_6\text{H}_3\text{Cl}_2)$, whose structure has been experimentally characterized by single-crystal XRD.¹⁰ In addition, the UV-vis-NIR spectra of its three structural isomers are available.¹⁰ This provides us with an opportunity to assign the detailed cage structures of some newly prepared mono-EMF derivatives by comparing their available UV-vis-NIR absorption spectra with that of the structurally characterized $\text{La}@C_{72}(\text{C}_6\text{H}_3\text{Cl}_2)$. Note that three regioisomers of $\text{La}@C_{72}(\text{C}_6\text{H}_3\text{Cl}_2)$ were isolated in the process of extracting $\text{La}@C_{72}$ -containing soot with 1,2,4-trichlorobenzene (TCB).¹⁰ Their differences are derived from different addition sites at the aryl ring of TCB. The three isomers with different dichlorophenyl radicals have been clearly characterized by ¹H NMR, while they were determined to possess a non-IPR cage structure, namely $\text{La}@C_{2v}(10612)-C_{72}$, by a combined single-crystal XRD and theoretical computation characterization.¹⁰

The metal Pr atom is interesting because it is similar in formal charge to La and it can be encapsulated into many fullerenes, such as C_{60} , C_{74} , C_{76} , C_{78} , C_{80} , C_{82} , to form mono-EMFs.^{46–48} In these Pr-containing mono-EMFs, only $\text{Pr}@C_{82}$ has been structurally characterized by XRD in a recent study by our group.⁴⁸ In this study, we attempt to prepare and isolate $\text{Pr}@C_{72}(\text{C}_6\text{H}_3\text{Cl}_2)$, a Pr counterpart of the structurally available molecule $\text{La}@C_{72}(\text{C}_6\text{H}_3\text{Cl}_2)$, and estimate its structure based on UV-vis-NIR and quantum mechanics data.

In addition, the pristine $\text{Pr}@C_{72}$ is also an interesting goal because the formation of the derivative $\text{Pr}@C_{72}(\text{C}_6\text{H}_3\text{Cl}_2)$ and the mass spectrometry (MS) data imply the existence of the pristine $\text{Pr}@C_{72}$ in soot. Although we did not isolate the underivatized $\text{Pr}@C_{72}$, some structural information is helpful for researchers to understand the nature of $\text{Pr}@C_{72}$. Therefore, in this study, we also provide the electronic structures, bonding nature, and metal-to-cage charge transfer of the pristine $\text{Pr}@C_{72}$ isomers with higher stability based on the quantum mechanics calculations.

2 Experimental section

2.1 General

Soot containing various empty fullerenes and Pr-EMFs was produced using a modified arc-discharge method under a 200 Torr helium atmosphere. The anode graphite rod was filled with

the PrNi_2 /graphite powder, while a pure graphite rod was employed as the cathode. Empty fullerenes and Pr-EMFs were extracted from soot with TCB at 486.65 K under an argon atmosphere for 15 h. After evaporating TCB, the dry soluble extract was added to a certain amount of toluene to perform further multi-stage separation *via* high performance liquid chromatography (HPLC, Japan Analytical Industry Corp. Ltd, Tokyo, Japan). The entire isolation process involved two types of Cosmosil columns (ϕ 20 mm \times 250 mm, Nacalai Tesque Inc., Kyoto, Japan), namely 5PYE and Buckyprep-M, with toluene as the eluent at different flow rates, while the 330 nm UV light was used for detection. In addition, the purity of the target product was analyzed by analytical HPLC (Hitachi High-Technologies Corp., Tokyo, Japan) with four different chromatographic columns (ϕ 4.6 mm \times 250 mm, Nacalai Tesque Inc., Kyoto, Japan), including Buckyprep-M, Buckyprep, 5PYE, and 5PBB.

Then, a composition determination for the target product was conducted by laser desorption ionization time-of-flight mass spectrometry (LDI-TOF MS) and matrix-assisted laser desorption ionization time-of-flight mass spectrometry (MALDI-TOF MS) with 1,1,4,4-tetraphenyl-1,3-butadiene as the matrix on a Bruker BIFLEX-III mass spectrometer (Bruker Corp., Bremen, Germany). The MS measurements were performed in the positive ion mode with toluene as the solvent, and the scan was over the range of m/z 600 to 2000. The UV-vis-NIR absorption spectrum was measured using a UV-3600 spectrometer (Shimadzu Corp., Kyoto, Japan) with carbon disulfide as the solvent. In the UV-vis-NIR measurement, the detection wavelength varied from 400 to 2000 nm.

2.2 Theoretical details

Geometry optimizations for all of the stationary points were performed using the BLYP^{49,50} and B3LYP^{49,50} functionals. The 3-21G⁵¹ and 6-31G(d)⁵² basis sets were employed for the C, H, and Cl atoms and the MWB48⁵³ basis set for the Pr atom. Furthermore, for the Pr atom, the effective core potential (ECP) was considered.⁵⁴ All of the stationary point geometries were fully optimized without symmetry constraints. To test whether the optimized structures are true minima, additional vibrational frequency calculations were performed at the B3LYP/6-31G(d)~MWB48 level of theory. The Mulliken charges, obtained by the single-point calculations using the B3LYP/6-31G(d)~MWB48-optimized geometries with the B3LYP and M06-2X functionals⁵⁵ and different basis sets (MWB,⁵³ CEP-4G,⁵⁶ and SDD⁵⁷ for metal atoms; 3-21G and 6-31G(d) for nonmetal atoms), were used to evaluate the metal-to-cage charge transfers. Furthermore, a natural bond orbital (NBO) analysis⁵⁸ was conducted to characterize the charge transfers and electronic configurations of the metal atoms at the B3LYP/3-21G~SDD and B3LYP/6-31G(d)~SDD levels of theory. To elucidate the addition sites to form metallofullerene derivatives, the π -orbital axis vector (POAV)^{59,60} pyramidalization angles of the pristine metallofullerene $\text{Pr}@C_{72}$ were computed using the B3LYP/6-31G(d)~MWB48-optimized geometry.

Generally, the abundances of EMF isomers are temperature-dependent. Because EMFs are formed at the very high temperatures of electric arc, we performed an additional temperature-dependent

computation on some of the isomers to estimate their thermodynamic distribution in line with the condition of the isomeric thermodynamic equilibrium. For a mixture consisting of n molecules, the mole fraction (x_i) of the isomer i can be computed through the partition function (q_i) and the ground-state energies (ΔE_i , 0 K), and the expression can be written as follows:

$$x_i = \frac{q_i \exp\left[\frac{-\Delta E_i}{RT}\right]}{\sum_{j=1}^n q_j \exp\left[\frac{-\Delta E_j}{RT}\right]} \quad (1)$$

where R is the gas constant, and T corresponds to the absolute temperature.⁶¹

Furthermore, the binding energy (BE) of a mono-EMF Pr@C_{2n} can be defined as the difference between the total energy ($E(\text{Pr}@C_{2n})$) of the mono-EMF Pr@C_{2n} and the sum of the total energies of the lowest-lying empty cage ($E(C_{2n})$) and a free Pr atom ($E(\text{Pr})$). Thus, it can be expressed as follows:

$$\text{BE} = E(\text{Pr}@C_{2n}) - E(C_{2n}) - E(\text{Pr}) \quad (2)$$

3 Results and discussion

3.1 Experiments

3.1.1 Isolation. As shown in Fig. 1a, the TCB extract containing Pr-EMFs, dichlorophenyl derivatives, and empty-cage fullerenes was roughly divided into nine fractions at the first HPLC stage. The highlighted broad fraction (Fr. 1), including the target product Pr@C₇₂(C₆H₃Cl₂), as well as other Pr-EMFs (Pr₂C₇₂, Pr₂C₈₀, etc.), dichlorophenyl derivatives (Pr@C₇₄(C₆H₃-Cl₂), Pr@C₇₆(C₆H₃Cl₂), Pr@C₈₀(C₆H₃Cl₂), etc.), and empty-cage fullerenes (C₇₀, C₇₆, C₇₈, etc.), was subjected to the second stage of separation to collect Fr. 2 (Fig. 1b). Then, Fr. 2 was

subjected to the third stage of separation to collect Fr. 3 (Fig. 1c), and Fr. 3 was subjected to the fourth stage of separation to collect Fr. 4 (Fig. 1d). Finally, the target product was isolated at the fifth stage of separation (Fig. 1e). The purity of the product was confirmed by analytical HPLC on varying columns. Fig. 2 shows the analytical HPLC plots of the product on Buckyprep-M, Buckyprep, 5PYE, and 5PBB columns. It is estimated from Fig. 2 that the purity of the product is more than 98%.

3.1.2 Molecular composition and UV-vis-NIR absorption spectrum. Fig. 3 demonstrates the MALDI-TOF MS and LDI-TOF MS of the product. The MALDI-TOF MS (Fig. 3a) displays a single peak at m/z 1150, and the isotropic distribution agrees perfectly with the calculated result of Pr@C₇₂(C₆H₃Cl₂) (insets in Fig. 3a), verifying the covalent attachment of the C₆H₃Cl₂ moiety onto the fullerene cage. The absence of fragmentation peaks reflects the high stability of the derivative, even under laser irradiation. Furthermore, the LDI-TOF MS (Fig. 3b) shows a single peak at m/z 1005, and the isotropic distribution agrees perfectly with the calculated result of Pr@C₇₂ (insets in Fig. 3b). It is apparent that the detected Pr@C₇₂ originates from the fragmentation of the monoadduct Pr@C₇₂(C₆H₃Cl₂) because of the absence of a matrix in the LDI-TOF MS. Thus, the above mass spectrometric studies verify the successful formation of the 1 : 1 dichlorophenyl monoadduct, yielded *via* the reaction of the mono-EMF Pr@C₇₂ in soot with the solvent TCB in the extraction procedure. In addition, no impurity peaks are detected in Fig. 3, confirming again the high purity of the isolated product.

UV-vis-NIR absorption spectroscopy is a powerful tool to characterize the geometries of the carbon cages of EMFs.^{13,62} Normally, the EMFs or their adducts with the same cage symmetry and formal charge have similar optical absorption spectra and *vice versa*,^{63–65} although the differences are in the metal or added species.^{66,67} Generally, this method must be combined with a quantum chemistry computation to more accurately confirm the cage structure of an EMF or its adduct.

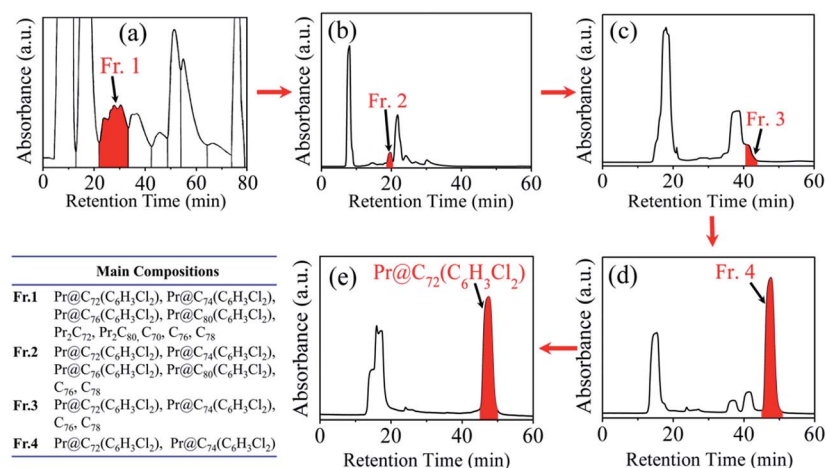


Fig. 1 Multi-stage HPLC separation/isolation scheme for Pr@C₇₂(C₆H₃Cl₂) and main compositions in all highlighted Frs. in red. (a) The first-step separation (5PYE column; flow rate 10.0 mL min⁻¹), (b) the second-step separation (Buckyprep-M column; flow rate 10.0 mL min⁻¹), (c) the third-step separation (Buckyprep-M column; flow rate 5.0 mL min⁻¹), (d) the fourth-step separation (5PYE column; flow rate 5.0 mL min⁻¹) and (e) the fifth-step separation (5PYE column; flow rate 5.0 mL min⁻¹). In the entire separation, toluene was used as the eluent, the detection wavelength was 330 nm, and the temperature was room temperature.

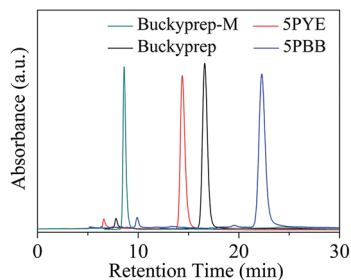


Fig. 2 Purity check of $\text{Pr@C}_{72}(\text{C}_6\text{H}_3\text{Cl}_2)$ by analytical HPLC using different columns with toluene as the eluent. In the analytical HPLC experiments, the flow rate was 1.0 mL min^{-1} , the detecting wavelength was 330 nm, and the temperature was 298.15 K.

Fig. 4 is the UV-vis-NIR absorption spectrum of $\text{Pr@C}_{72}(\text{C}_6\text{H}_3\text{Cl}_2)$ in which two strong characteristic peaks at 659 and 1068 nm along with three slightly weak peaks at 450, 532 and 945 nm are observed. Interestingly, these features are similar to those reported previously for the three regioisomers (A, B, and C, see Fig. 4) of the dichlorophenyl derivative $\text{La@C}_{72}(\text{C}_6\text{H}_3\text{Cl}_2)$.¹⁰ It should be noted that only the structure A, which is not the highest yield among the three isomers, is structurally characterized by single-crystal XRD.¹⁰ However, in the present case, only one positional isomer was isolated. Therefore, we can reasonably conclude that the isolated $\text{Pr@C}_{72}(\text{C}_6\text{H}_3\text{Cl}_2)$ should be the lowest-lying structure. Based on the fact that the three $\text{La@C}_{72}(\text{C}_6\text{H}_3\text{Cl}_2)$ isomers (A, B, and C) prove to be of the same cage structure ($\text{C}_2(10612)\text{-C}_{72}$)¹⁰ and that the UV-vis-NIR absorption spectra of the three $\text{La@C}_{72}(\text{C}_6\text{H}_3\text{Cl}_2)$ isomers and the present $\text{Pr@C}_{72}(\text{C}_6\text{H}_3\text{Cl}_2)$ are very similar (Fig. 4), it is reasonable for us to tentatively ascribe the carbon cage of $\text{Pr@C}_{72}(\text{C}_6\text{H}_3\text{Cl}_2)$ as that of $\text{La@C}_{72}(\text{C}_6\text{H}_3\text{Cl}_2)$, *i.e.*, $\text{C}_2(10612)\text{-C}_{72}$. The relevant theoretical evidence in support of the determination will be given in the next section.

3.2 Theoretical estimation of the structure of $\text{Pr@C}_{72}(\text{C}_6\text{H}_3\text{Cl}_2)$

Previous reports proposed that the carbon atoms at adjacent pentagon pairs (APPs) of endohedral fullerenes are more reactive than others;^{10,40} hence, they may be the preferred reaction

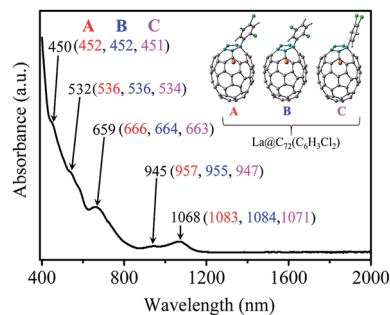


Fig. 4 UV-vis-NIR absorption spectrum of the purified sample of $\text{Pr@C}_{72}(\text{C}_6\text{H}_3\text{Cl}_2)$ in carbon disulfide solution. The corresponding absorption peaks of three $\text{La@C}_{72}(\text{C}_6\text{H}_3\text{Cl}_2)$ isomers (A, B, C) were taken from ref. 10 and are shown in parentheses in different colors.

sites for exohedral chemical functionalization of Pr@C_{72} by an addition reaction with TCB, as exemplified in the reaction of La@C_{72} with TCB.¹⁰ To theoretically determine the preferable addition positions, we computed the distribution of the unpaired electron and π -orbital axis vector (POAV) pyramidalization angles of all of the C atoms in $\text{Pr@C}_2(10612)\text{-C}_{72}$. The latter is an effective index of the bond strain of fullerenes. Both the spin density and POAV pyramidalization angles have been widely used to estimate potential reactive sites in the exohedral chemical functionalization of paramagnetic EMFs.^{10,68-71} Generally, a reactive site should possess relatively high spin density and POAV values, and the determination should integrate the two aspects.^{10,12} The computed results of the spin densities and POAV pyramidalization angles listed in Table S1 (see the ESI[†]) indicate that the carbon atoms in APPs possess relatively high POAV and spin density values as compared with other carbon atoms. Due to the limitation of cage symmetry, only four types of carbon atoms exist at the APPs, and the representative atoms C(66), C(68), C(70), and C(71) were used in computations and discussion. After the addition of Pr@C_{72} to TCB, three different dichlorophenyl free radicals (2,4-, 2,5-, and 3,4-dichlorophenyl radicals) are possible; thus, twelve regioisomers are expected. Further considering two possible conformations derived from two different orientations of the aryl ring in each regioisomer, twenty-four isomers should be

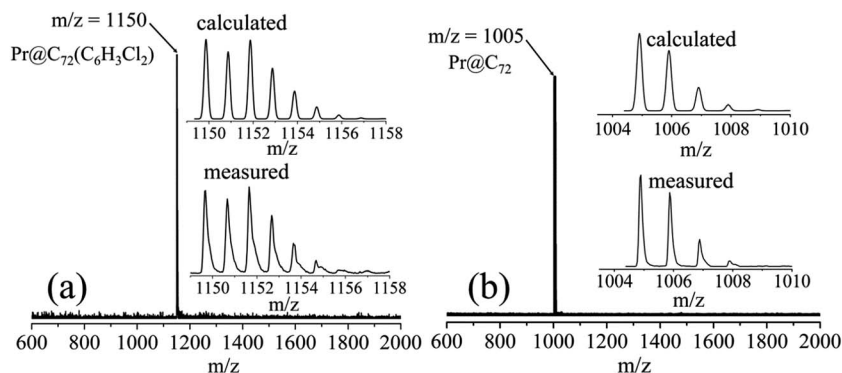


Fig. 3 (a) MALDI-TOF mass spectrum obtained with 1,1,4,4-tetraphenyl-1,3-butadiene as the matrix and (b) LDI-TOF mass spectrum. In the experiments, the positive-ion mode was used. The insets show the measured and calculated isotope distributions.

theoretically predicted for $\text{Pr}@C_{72}(\text{C}_6\text{H}_3\text{Cl}_2)$. The geometries and relative energies of the optimized twenty-four $\text{Pr}@C_{72}(\text{C}_6\text{H}_3\text{Cl}_2)$ isomers are shown in Fig. S1 and Table S2 (see the ESI[†]), respectively. Based on the computed data, we can readily find that the six isomers with different dichlorophenyl radicals linked to C(70) are lower lying. The higher addition activity of C(70) can be rationalized by the relatively high spin density (0.08) and POAV value (13.11) compared with those of other carbon atoms (see Table S1[†]).

To obtain more accurate relative energies, we further optimized the six low-lying isomers at the B3LYP/6-31G(d)~MWB48 level of theory, and the computed results are shown in Fig. 5. The results show that the relative energies of **1c** (0.00 kcal mol⁻¹) and **1c'** (0.15 kcal mol⁻¹) with the 3,4-dichlorophenyl substituent are the lowest energy structures, followed by **1b** (1.22 kcal mol⁻¹), **1a** (1.35 kcal mol⁻¹), **1b'** (2.69 kcal mol⁻¹), and **1a'** (2.73 kcal mol⁻¹). Furthermore, after considering the Gibbs free energy correction to the total energies, we predict that the total thermodynamic distributions of **1c** and **1c'** reach 96% and 92% at 298.15 and 486.65 K (see Fig. 5 and Table S3 in the ESI[†]), respectively, and the concentrations of the other four isomers are low. Because we obtained only one extraction in the process of extracting $\text{Pr}@C_{72}$ with TCB, the products should be the conformational isomers **1c** and **1c'** with the equilibrium concentration distributions of 7.4 : 10 and 7 : 10 at 298.15 and 486.65 K (Table S3[†]), respectively.

Furthermore, the optimized carbon cage of the bare $\text{Pr}@C_{72}$ is $C_2(10612)-C_{72}$ with C_2 symmetry. After forming the mono-adducts **1c** and **1c'**, the molecular symmetries changed to C_1 . In addition, the positions of the Pr atoms in **1c** and **1c'** are significantly different from the pristine $\text{Pr}@C_{72}$; it can be observed that the position clearly deviates from the C_2 axis (see the geometric data in the ESI[†]). The detailed structure of $\text{Pr}@C_{72}$ is provided in the next section.

When the similarity in the UV-vis-NIR absorption spectrum is used to determine whether a new EMF or derivative and a structurally characterized counterpart (the reference molecule) bear the same carbon cage, two preconditions must be fulfilled, *i.e.*, there must be identical charge states (formal or quantum mechanics charge) for the encapsulated metal atoms and there must be a negligible contribution of metal atoms to the orbitals that are closely correlated to the UV-vis-NIR absorption spectra. The former determines that the two

carbon cage isomers bear the same negative charge, while the latter ensures that the UV-vis-NIR absorption spectra are associated with only the carbon cages. Because a UV-vis-NIR spectrum can provide information regarding the low-energy electron excitations associated with the $\pi-\pi^*$ transition of the carbon cage, the orbitals in the second precondition involve only those that are adjacent to the frontier molecular orbitals (FMOs).

We computed the Mulliken charges of the metal atoms in $\text{Pr}@C_2(10612)-C_{72}(\text{C}_6\text{H}_3\text{Cl}_2)$ (**1c**) and its La counterpart, $\text{La}@C_2(10612)-C_{72}(\text{C}_6\text{H}_3\text{Cl}_2)$ (**C**), at the various levels of theory. The results listed in Table 1 indicate that the charges of the Pr and La atoms in the corresponding mono-EMF derivatives are very close at the same computational level. Furthermore, for **1c** or **C**, although the metal charges computed using the 3-21G basis set are significantly higher than those using the 6-31G(d) basis set, the B3LYP and M06-2X functionals give very close metal charges when the same basis set is employed. All of these results imply that the Pr and La atoms in $\text{M}@C_2(10612)-C_{72}(\text{C}_6\text{H}_3\text{Cl}_2)$ ($\text{M} = \text{Pr}, \text{La}$) should have the same charges.

To accurately complete the comparison of $\text{Pr}@C_2(10612)-C_{72}(\text{C}_6\text{H}_3\text{Cl}_2)$ with its La analogue, we computed their relevant molecular orbitals. The computed orbitals were plotted in Table S4 (see the ESI[†]), from which we can directly observe no contribution of Pr or La to these orbitals. Therefore, the UV-vis-NIR spectra of the $\text{M}@C_2(10612)-C_{72}(\text{C}_6\text{H}_3\text{Cl}_2)$ ($\text{M} = \text{Pr}, \text{La}$) molecules are associated only with the C_{72} cage. Considering the satisfactory fulfillment of the two preconditions and the similarity in the UV-vis-NIR spectrum compared with the reference system $\text{La}@C_2(10612)-C_{72}(\text{C}_6\text{H}_3\text{Cl}_2)$, we can reasonably conclude that the isolated $\text{Pr}@C_{72}(\text{C}_6\text{H}_3\text{Cl}_2)$ possesses a $C_2(10612)-C_{72}$ cage.

3.3 Theoretical evaluation of $\text{Pr}@C_{72}$

3.3.1 Geometries and energies. Because the fullerene C_{72} possesses many configurations,³⁴ there must be a great number of structural isomers with different cage structures and metal endohedral positions after the encapsulation of Pr inside of the

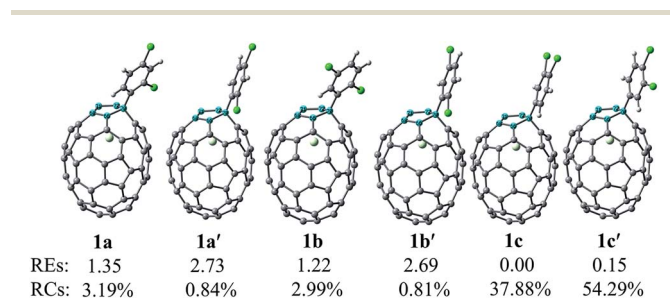


Fig. 5 Optimized structures, relative energies (REs, kcal mol⁻¹, 0 K), and relative concentrations (RCs, 486.65 K) of $\text{Pr}@C_2(10612)-C_{72}(\text{C}_6\text{H}_3\text{Cl}_2)$ at the B3LYP/6-31G(d)~MWB48 level of theory.

Table 1 Computed Mulliken charges of $\text{Pr}@C_{72}(\text{C}_6\text{H}_3\text{Cl}_2)$ (**1c**) and $\text{La}@C_{72}(\text{C}_6\text{H}_3\text{Cl}_2)$ (**C**) using the B3LYP and M06-2X functionals with the 3-21G and 6-31G(d) (for the Cl, C, and H atoms), MWB48 (for the Pr atom), MWB46 (for the La atom), and CEP-4G and SDD (for the Pr, La atom) basis sets

Methods	Basis sets	$\text{Pr}@C_2(10612)-C_{72}(\text{C}_6\text{H}_3\text{Cl}_2)$ (1c)	$\text{La}@C_2(10612)-C_{72}(\text{C}_6\text{H}_3\text{Cl}_2)$ (C) ^a
B3LYP	3-21G~MWB	2.77	2.86
	3-21G~SDD	2.63	2.85
	6-31G(d)~MWB	0.89	0.95
	6-31G(d)~CEP-4G	1.24	1.21
	6-31G(d)~SDD	0.79	0.73
M06-2X	3-21G~MWB	2.63	2.73
	3-21G~SDD	2.39	2.57
	6-31G(d)~MWB	0.95	1.03
	6-31G(d)~CEP-4G	1.25	1.32
	6-31G(d)~SDD	0.73	0.64

^a The structure of $\text{La}@C_2(10612)-C_{72}(\text{C}_6\text{H}_3\text{Cl}_2)$ (**C**) is given in Fig. 4.

C_{72} cage. It appears that it is nearly impossible to explore all of the possible isomers. To locate the low-lying isomers of an EMF with the formal charge distribution of $M^{q+}@C_{2n}^{q-}$, the following method was frequently used in previous investigations.^{14,17,72} First, geometry optimizations should be conducted for the negatively charged C_{2n}^{q-} using the geometries of all of the IPR and partial non-IPR isomers of C_{2n} . Then, the resulting low-lying configurations are encapsulated with the metal atom M to initialize the models of $M@C_{2n}$, followed by further optimization to locate the geometries of stationary points. Using this approach, the low-lying isomers of $M@C_{2n}$ can be obtained.

For the fullerene C_{72} , 11190 isomers including only one IPR structure have been predicted based on the spiral algorithm proposed by Fowler and Manolopoulos.³⁴ In this study, we selected the IPR-satisfying C_{72} cage and some non-IPR structures with APPs less than three as targets. Generally, fewer APPs of a C_{2n} cage indicate that it has a lower energy. Because the encapsulated Pr atom can transfer less than three electrons to the carbon cage, we initially compute the energies of the selected C_{72} cages and the corresponding C_{72}^{-} , C_{72}^{2-} , and C_{72}^{3-} anions. The calculated relative energies at the different levels of theory, as well as those of the structural isomers of $Pr@C_{72}$, are listed in Table S5 (see the ESI[†]), while the relative energy dependence of C_{72} , C_{72}^{3-} , and $Pr@C_{72}$ on the carbon cage and computational level are shown in Fig. 6. Although the IPR anions $D_{6d}(11190)-C_{72}^{n-}$ ($n = 1-3$) and $Pr@C_{72}(11190)$ are relatively high lying, they are provided in Table S5[†] to complete a comparison with the non-IPR isomers. The computations were mainly performed at the BLYP/3-21G~MWB48 level of theory, and further expensive computations were conducted at the B3LYP/6-31G(d)~MWB48 level of theory for only the three lowest-lying species, $Pr@C_{2v}(11188)-C_{72}$, $Pr@C_s(10528)-C_{72}$, and $Pr@C_2(10612)-C_{72}$. The results in Table S5[†] and Fig. 6 indicate that the energy ordering and energy differences of $Pr@C_{2v}(11188)-C_{72}$, $Pr@C_s(10528)-C_{72}$, and $Pr@C_2(10612)-C_{72}$ at the BLYP/3-21G~MWB48 level of theory are in good agreement with these computed at the B3LYP/6-31G(d)~MWB48 level of theory. Therefore, it is reasonable to conclude that the isomers $Pr@C_{2v}(11188)-C_{72}$, $Pr@C_s(10528)-C_{72}$, and $Pr@C_2(10612)-C_{72}$

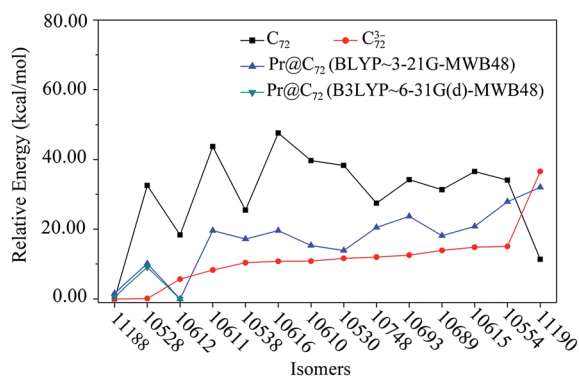


Fig. 6 Relative energies of optimized C_{72} , C_{72}^{3-} , and $Pr@C_{72}$ at different levels of computation. The fullerene isomers are coded according to the spiral algorithm, which was proposed by Fowler and Manolopoulos, see ref. 34.

with the molecular symmetries of C_{2v} , C_1 , and C_2 , respectively, are the three lowest-lying configurations. Furthermore, additional computations indicate that the isomers $Pr@C_2(10612)-C_{72}$ and $Pr@C_{2v}(11188)-C_{72}$ with the multiplicity of four (quartet) are higher in energy than their respective structures with the multiplicity of two (doublet) by 33.42 and 20.78 kcal mol⁻¹ (Table S6[†]), respectively. Therefore, the ground state structures of $Pr@C_2(10612)-C_{72}$ and $Pr@C_{2v}(11188)-C_{72}$ are doublets.

As discussed above, after encapsulating a Pr atom into the C_{72} cage, the resulting $Pr@C_2(10612)-C_{72}$ is predicted as the most thermodynamically stable isomer, followed by the non-IPR structure $Pr@C_{2v}(11188)-C_{72}$ with a relative energy of only 0.62 kcal mol⁻¹ (Table S5[†]). This situation is similar to analogues with different metals M (M = La,^{10,73-75} Ca,^{76,77} Eu,⁷⁸ Yb⁷²) from the available DFT computations, as listed in Table 2.

In the present study, another non-IPR isomer $Pr@C_s(10528)-C_{72}$ is higher in energy than the lowest-lying $Pr@C_2(10612)-C_{72}$ by 9.03 kcal mol⁻¹. Such a high relative energy indicates that the isolation of $Pr@C_s(10528)-C_{72}$ is nearly impossible compared with $Pr@C_2(10612)-C_{72}$ and $Pr@C_{2v}(11188)-C_{72}$ with higher thermodynamic stabilities.

Considering that there is only a 0.62 kcal mol⁻¹ energy difference between $Pr@C_2(10612)-C_{72}$ and $Pr@C_{2v}(11188)-C_{72}$, it appears that the two isomers should coexist in the experiments. We evaluated their thermodynamic probabilities from 273 to 4000 K based on eqn (1). The results plotted in Fig. 7 indicate that the relative concentrations of $Pr@C_2(10612)-C_{72}$ and $Pr@C_{2v}(11188)-C_{72}$ are 95 : 5 at 500 K. With an increasing temperature, the concentration of $Pr@C_2(10612)-C_{72}$ decreases gradually, and the concentration of $Pr@C_{2v}(11188)-C_{72}$

Table 2 Computed relative energies (kcal mol⁻¹) of $M@C_2(10612)-C_{72}$ and $M@C_{2v}(11188)-C_{72}$ (M = La, Ca, Eu, Yb, Pr). The shortest M–C bond lengths (Å) and molecular symmetries in those molecules are provided in square brackets

M	Level	Ref.	$M@C_2$ (10612)- C_{72}	$M@C_{2v}$ (11188)- C_{72}
La	B3LYP/6-31G(d) ~LANL2DZ	75	0.00	0.26
	BLYP/DNP	73	[2.57, C_2]	
	PW91/DNP	74	[2.586, C_2]	
	B3LYP/6-31G(d)	10	[2.605, 2.680, C_2]	
Ca	B3LYP/6-31G~(5s5p)/ [4s4p] ^a	76	0.00[C_2]	1.20[C_{2v}]
	B3P/6-31G~(5s5p)/ [4s4p] ^a	76	0.00[C_2]	1.60[C_{2v}]
	B3LYP/6-31G~dz ^b	77	0.00	0.80
	B3LYP/6-31G(d) ^b	77	0.00	0.04
Eu	PW91/DNP	78	[2.57]	
Yb	B3LYP/6-31G(d) ~CEP-4G	72	1.80 [2.638, C_2]	0.00 [2.571, C_{2v}]
Pr	B3LYP/6-31G(d) ~MWB48	This study	0.00 [2.565, C_2]	0.62 [2.527, C_{2v}]

^a Single-point computations with the HF/3-21G-dz-optimized geometries.

^b Single-point computations with the B3LYP/3-21G-dz-optimized geometries.

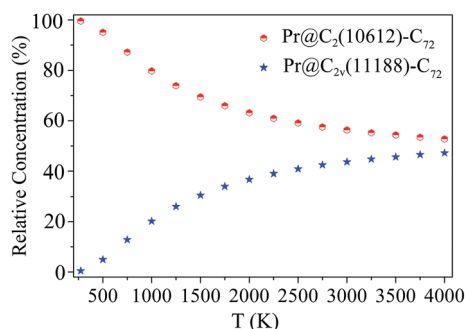


Fig. 7 Relative concentrations (RCs) of Pr@C₂(10612)-C₇₂ and Pr@C_{2v}(11188)-C₇₂. The Gibbs free energy corrections were performed by single-point computations at the BLYP/3-21G~MWB48 level with the B3LYP/6-31G(d)~MWB48-optimized geometries.

increases gradually. When the temperature reaches 2000 and 4000 K, their ratios are 63 : 37 and 53 : 47, respectively.

The optimized structures of Pr@C₂(10612)-C₇₂ and Pr@C_{2v}(11188)-C₇₂ as well as the characteristic [5,5] bonds and the corresponding C-Pr bond distances are shown in Fig. 8, while their detailed structural information is provided in the ESI.† According to the computational results, we can assign the symmetry of isomer Pr@C₂(10612)-C₇₂ as C₂ symmetry, which is similar to the corresponding empty-cage C₇₂ (C₂(10612)-C₇₂). In Pr@C₂(10612)-C₇₂, the Pr atom is found to localize along the C₂ axis, which crosses the midpoint of the [5,5] bond (Fig. 8a). Therefore, the Pr atom is equidistant from the endpoints of the [5,5] bond. The corresponding Pr-C bond lengths (2.565 Å) are the shortest among all of the Pr-C distances. Three M@C₇₂ (M = La, Ca, Yb) structures with C₂ symmetry have also been identified by theoretical computations^{10,73,74} and/or available experiments.¹⁰ As shown in Table 2 that the shortest M-C distances in La@C₂(10612)-C₇₂, Eu@C₂(10612)-C₇₂ and Yb@C₂(10612)-C₇₂ are 2.57–2.68 Å,^{10,73,74} 2.57 Å,⁷⁸ and 2.638 Å,⁷² respectively, which are very close to the shortest Pr-C bond length in Pr@C₂(10612)-C₇₂.

Similar to the position of the Pr atom in Pr@C₂(10612)-C₇₂, the Pr atom in Pr@C_{2v}(11188)-C₇₂ also localizes along the C₂ axis of C_{2v}(11188)-C₇₂, which crosses the midpoint of the [5,5] bond (Fig. 8b). The mono-EMF maintains the symmetry with the empty cage. The shortest Pr-C bond length, *i.e.*, the bond distance between the Pr atom and the endpoints of the [5,5] bond, is 2.527 Å, which is slightly shorter than that (2.565 Å) in

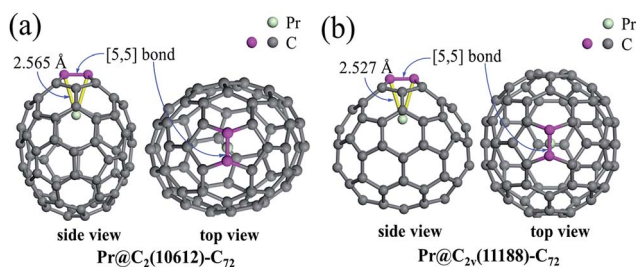


Fig. 8 Optimized structures of (a) Pr@C₂(10612)-C₇₂ and (b) Pr@C_{2v}(11188)-C₇₂ at the B3LYP/6-31G(d)-MWB48 level.

Pr@C₂(10612)-C₇₂. The pure carbon cage C_{2v}(11188)-C₇₂ is a very special cage because it possesses the lowest energy among all of the neutral C₇₂ isomers and the corresponding C₇₂²⁻ and C₇₂³⁻ are the most stable dianion and trivalent anions (Table S5†), respectively. However, to date, no experimental investigations of C_{2v}(11188)-C₇₂ as the main host to encapsulate metal atom(s) or a cluster are available.

3.3.2 Electron transfers and charges of metal atoms. The La atoms in the reference molecules La@C₂(10612)-C₇₂ and La@D_{3h}(14246)-C₇₄ have been theoretically verified to be in the 3+ states.^{10,74,79} In addition, the Pr and La atoms inside of the C₈₂ cage were suggested to be in the 3+ states by X-ray photoelectron spectroscopy (XPS).^{47,80} These results indicate that the formal charge of the La and Pr atoms in these EMFs is +3. Thus, M@C₈₂ (M = Pr, La) are also selected as reference systems in the following discussion.

The Mulliken charges of the target molecules Pr@C₂(10612)-C₇₂ and Pr@C_{2v}(11188)-C₇₂ and three reference systems (La@C₂(10612)-C₇₂ and M@C_{2v}-C₈₂ (M = Pr, La)) were computed at various levels of theory. Based on the computed results listed in Table 3, several features can be found. First, at the same computational level, the charges of the La and Pr atoms in all five La- and Pr-containing EMFs are very close, indicating that the metal atoms in these molecules should possess the same formal charges. Second, under the same basis set, the B3LYP and M06-2X functionals give similar charge values, and for most of the molecules, the former gives slightly higher charges than the latter. Last, although the 3-21G-computed charges (2.2–2.8e) are higher than the 6-31G(d) (0.6–1.4e) for the Pr atom, the charges obtained under the same basis set remain very close, indicating that the basis set selection has only a minor effect on the charge determination relative to a reference system. Further, we can note that the metal atoms in M@C₂(10612)-C₇₂(C₆H₃Cl₂) and M@C₂(10612)-C₇₂ (M = Pr, La) are in nearly equivalent charge states (see Tables 1 and 3) at the same basis set, indicating that the dichlorophenyl substituent has a negligible effect on the formal charges of the endohedral metal atoms. Based on the description above and the available charges (3+) in the reference molecules, we can reasonably consider the metal Pr atoms of Pr@C₂(10612)-C₇₂, Pr@C₂(10612)-C₇₂(C₆H₃Cl₂), and Pr@C_{2v}(11188)-C₇₂ to be in trivalent states.

The discussed formal charge states depend solely on the electron transfer from Pr to the carbon cage. In addition, the metal-to-cage electron transfer leads to the interaction and bonding between Pr and the carbon cage, which effectively stabilizes the C₇₂ cage. The computed natural electron configurations and NBO charges of metals for the target systems Pr@C₂(10612)-C₇₂ and Pr@C_{2v}(11188)-C₇₂ and the reference molecule Pr@C_{2v}-C₈₂ are summarized in Table 4. The Pr atoms donate 2.42–2.63e from the 4f and 6s orbitals to the carbon cages. However, it is surprising that the electron acceptor also provides a considerable amount of electrons (approximately 1.12–1.30e) to the higher-lying 5d, 6p and 6d orbitals of Pr, which was considered as a back-donation effect in previous studies.^{14,15,81} The donation and back-donation result in the low NBO charge of +1.16 to +1.51e relative to the formal charge of

Table 3 Computed Mulliken charges using the B3LYP and M06-2X functionals. The 3-21G and 6-31G(d) basis sets are for the C atom, the MWB48 basis set for the Pr atom, the MWB46 basis set for the La atom, and CEP-4G and SDD basis sets for the Pr and La atoms

Methods	Basis sets	Pr@C ₂ (10612)-C ₇₂	Pr@C _{2v} (11188)-C ₇₂	Pr@C _{2v} -C ₈₂	La@C ₂ (10612)-C ₇₂	La@C _{2v} -C ₈₂
B3LYP	3-21G~MWB	2.71	2.78	2.72	2.83	2.58
	3-21G~SDD	2.63	2.54	2.48	2.85	2.56
	6-31G(d)~MWB	0.88	0.98	1.06	0.96	1.06
	6-31G(d)~CEP-4G	1.28	1.12	1.33	1.27	1.21
	6-31G(d)~SDD	0.87	0.86	0.89	0.75	0.87
M06-2X	3-21G~MWB	2.60	2.65	2.61	2.71	2.46
	3-21G~SDD	2.39	2.31	2.29	2.56	2.30
	6-31G(d)~MWB	0.96	1.05	1.13	1.05	1.06
	6-31G(d)~CEP-4G	1.21	1.09	1.33	1.38	1.29
	6-31G(d)~SDD	0.64	0.79	0.88	0.64	0.81

Table 4 Computed natural electron configurations (NECs, in e), NBO charges (NCs, in e) on the Pr atom, summations of the lost electrons (LEs, in e) from 6s and 4f of the Pr atom, and total back donation of electrons (BDEs, in e) from cage to the Pr atom by the single-point calculations using the B3LYP/6-31G(d)~MWB48-optimized geometries with the B3LYP method and different basis sets

Systems	Basis sets	NECs	NCs	LEs	BDEs
Pr@C ₂ (10612)-C ₇₂	3-21G~SDD	6s ^{0.10} 4f ^{2.48} 5d ^{0.80} 6p ^{0.35} 6d ^{0.11}	1.16	2.42	1.26
	6-31G(d)~SDD	6s ^{0.09} 4f ^{2.44} 5d ^{0.87} 6p ^{0.33} 6d ^{0.10}	1.17	2.47	1.30
Pr@C _{2v} (11188)-C ₇₂	3-21G~SDD	6s ^{0.08} 4f ^{2.44} 5d ^{0.80} 6p ^{0.28} 6d ^{0.10}	1.30	2.48	1.18
	6-31G(d)~SDD	6s ^{0.07} 4f ^{2.43} 5d ^{0.85} 6p ^{0.26} 6d ^{0.08}	1.31	2.50	1.19
Pr@C _{2v} -C ₈₂	3-21G~SDD	6s ^{0.06} 4f ^{2.31} 5d ^{0.83} 6p ^{0.21} 6d ^{0.08}	1.51	2.63	1.12
	6-31G(d)~SDD	6s ^{0.05} 4f ^{2.33} 5d ^{0.86} 6p ^{0.21} 6d ^{0.07}	1.48	2.62	1.14

3+. Therefore, an electronic reorganization must occur after the Pr³⁺ ion is formed by the encapsulation of the Pr atom into these empty carbon cages. This makes the metal-cage bonding complex, as described in the following section.

3.3.3 Metal-cage orbital interactions. Fig. 9 and 10 show the two-dimensional (2D) and three-dimensional (3D) fragmental electron density differences of Pr@C₂(10612)-C₇₂ and

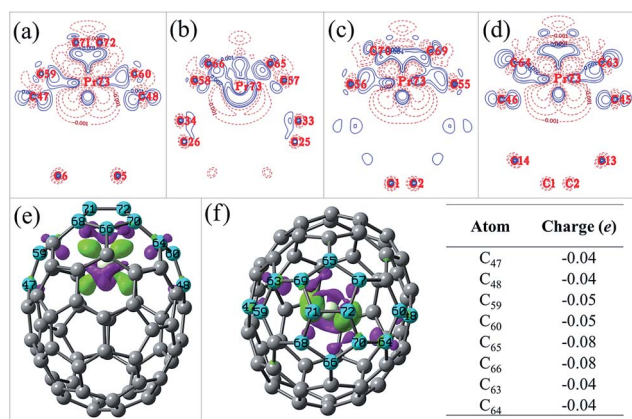


Fig. 9 Fragmental electron difference densities of Pr@C₂(10612)-C₇₂. (a) C₇₁-C₇₂-Pr₇₃ 2D plane, (b) C₆₅-C₆₆-Pr₇₃ 2D plane, (c) C₆₉-C₇₀-Pr₇₃ 2D plane, (d) C₆₃-C₆₄-Pr₇₃ 2D plane, (e) 3D (side view), and (f) 3D (top view) and the charges of partial carbon atoms. Blue solid lines (or purple regions) and brown dotted lines (or green regions) show the increase and decrease in electron density, respectively. Blue balls represent the C atoms with a relatively strong interaction with the Pr atom. Three-dimensional (3D) fragmental difference densities are plotted with an isodensity value of 0.008 hartree.

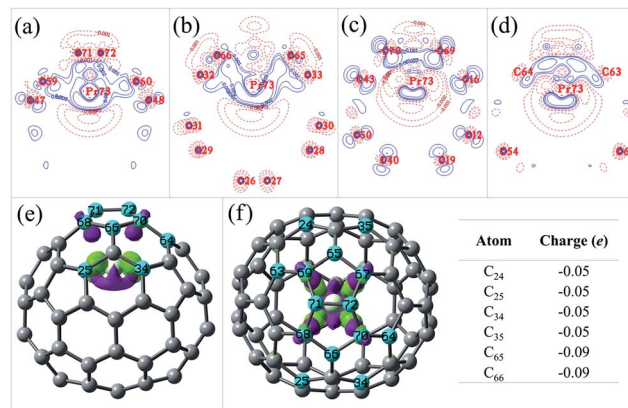


Fig. 10 Fragmental difference densities of Pr@C_{2v}(11188)-C₇₂. (a) C₇₁-C₇₂-Pr₇₃ 2D plane, (b) C₆₅-C₆₆-Pr₇₃ 2D plane, (c) C₆₉-C₇₀-Pr₇₃ 2D plane, (d) C₆₃-C₆₄-Pr₇₃ 2D plane, (e) 3D (side view), and (f) 3D (top view) and the charges of partial carbon atoms. Blue solid lines (or purple regions) and brown dotted lines (or green regions) show the increase and decrease in electron density, respectively. Blue balls represent the C atoms with a relatively strong interaction with the Pr atom. Three-dimensional (3D) fragmental difference densities are plotted with an isodensity value of 0.008 hartree.

Pr@C_{2v}(11188)-C₇₂, respectively, while the electron density differences of C₂(10612)-C₇₂ and C_{2v}(11188)-C₇₂ are provided in Fig. S2.† As shown in the contour maps (Fig. 9a–d) and in the isosurface views (Fig. 9e and f) of Pr@C₂(10612)-C₇₂, the electron density around the Pr atom decreases, which implies a metal-to-cage electron transfer. The excess electron density localizes mainly at the C(65) and C(66) atoms of the cage pole

and other several carbon atoms of the equatorial region, as indicated in the inset table in Fig. 9f. The contour and isosurface graphs reflect not only the strong interaction between Pr and the carbon atoms at the cage pole (the eight carbon atoms of APPs) and cage equator (C(63) and C(64)) but also the slightly weak orbital interaction between Pr and the equatorial carbon atoms, involving mainly C(59), C(60), C(47), and C(48). However, in Pr@C_{2v}(11188)-C₇₂, only the strong bonding between Pr and four polar carbon atoms, C(69), C(68), C(67), and C(70), can be observed (Fig. 10a–f). The more complex metal–cage interaction in Pr@C₂(10612)-C₇₂ can be attributed to the relatively long and narrow configuration of Pr@C₂(10612)-C₇₂; however, the absence of metal–cage bonding in Pr@C_{2v}(11188)-C₇₂ associated with the equatorial carbon atoms is due to the relatively large distance between Pr and the cage equator, resulting from the fattened shape of Pr@C_{2v}(11188)-C₇₂ (Fig. 10e and f).

An additional computation of the BEs of Pr@C₂(10612)-C₇₂ and Pr@C_{2v}(11188)-C₇₂ based on eqn (2) indicates that the B3LYP/6-31G(d)~MWB48-computed BEs are -72.07 and -53.15 kcal mol⁻¹ for Pr@C₂(10612)-C₇₂ and Pr@C_{2v}(11188)-C₇₂, respectively. Because the relaxations among different low-lying empty cages require less than 20 kcal mol⁻¹ in thermodynamic energy, we can reasonably conclude that Pr@C₂(10612)-C₇₂ has a larger metal–cage interaction energy than Pr@C_{2v}(11188)-C₇₂. This can be rationalized by the cooperative action of the metal–carbon (at the polar region) and metal–carbon (near the equator) interactions in Pr@C₂(10612)-C₇₂. In addition, a much narrower molecular shape of Pr@C₂(10612)-C₇₂ than Pr@C_{2v}(11188)-C₇₂ should be responsible for the low BE of Pr@C₂(10612)-C₇₂.

4 Conclusions

In this study, we successfully synthesized a novel Pr-containing mono-EMF derivative, Pr@C₇₂(C₆H₃Cl₂). The monoadduct was generated in the process of extracting the soot with TCB and was isolated from various empty fullerenes and endohedral fullerenes or dichlorophenyl derivatives by a multi-stage HPLC procedure. The purity of the sample was checked by analytical HPLC. The molecular composition of monoadduct Pr@C₇₂(C₆H₃Cl₂) was confirmed by MALDI-TOF mass spectrometry. Furthermore, we found that the UV-vis-NIR absorption spectrum of Pr@C₇₂(C₆H₃Cl₂) is very similar to those of the three isomers of the La-containing mono-EMF derivative La@C₂(10612)-C₇₂(C₆H₃Cl₂). By further considering the quantum mechanics results, we confirm that the structure of the novel mono-EMF derivative Pr@C₇₂(C₆H₃Cl₂) is Pr@C₂(10612)-C₇₂(C₆H₃Cl₂).

In addition, we investigated the properties of the pristine Pr@C₇₂. Pr@C₂(10612)-C₇₂ and Pr@C_{2v}(11188)-C₇₂ are predicted to be the most energetically favorable structures of all of the Pr@C₇₂ isomers, and their energy difference is only 0.62 kcal mol⁻¹ in favor of Pr@C₂(10612)-C₇₂. The relative concentrations of Pr@C₂(10612)-C₇₂ and Pr@C_{2v}(11188)-C₇₂ are 95 : 5, 63 : 37, and 53 : 47 at 500, 2000, and 4000 K, respectively. The Pr atoms in Pr@C₂(10612)-C₇₂, Pr@C_{2v}(11188)-C₇₂, and the adduct Pr@C₇₂(C₆H₃Cl₂) are in the 3+ formal charge states. For Pr@C₂(10612)-C₇₂, the electron acceptor (carbon cage) provides

a considerable amount of electrons to the higher-lying 5d, 6p and 6d orbitals of Pr; thus, an obvious back-donation effect exists in the interaction of the metal atom Pr and the carbon cage.

The combination of the theoretical simulation and the experiment allows us to reasonably identify and rationalize the structures of the aforementioned Pr-containing mono-EMF dichlorophenyl derivative Pr@C₇₂(C₆H₃Cl₂) and mono-EMF Pr@C₇₂. This study effectively extends the family of the Pr-based mono-EMFs and their derivatives. For Pr@C₇₂(C₆H₃Cl₂) and Pr@C₇₂, further experiments are required for isolation and the subsequent structural characterization (for example, NMR and single-crystal XRD).

Acknowledgements

This research was supported by the National Natural Science Foundation of China (Grants 21173072, 21271067) and the Program for Innovative Research Team in University (The Ministry of Education of China, Grant IRT-1237).

References

- 1 K. Kobayashi and S. Nagase, in *Endofullerenes: A New Family of Carbon Cluster*, ed. T. Akasaka and S. Nagase, Springer, Dordrecht, 2002, pp. 99–119.
- 2 M. N. Chaur, A. J. Athans and L. Echegoyen, *Tetrahedron*, 2008, **64**, 11387–11393.
- 3 M. N. Chaur, F. Melin, A. L. Ortiz and L. Echegoyen, *Angew. Chem., Int. Ed.*, 2009, **48**, 7514–7538.
- 4 L. Dunsch and S.-F. Yang, *Phys. Chem. Chem. Phys.*, 2007, **9**, 3067–3081.
- 5 X. Lu, L. Feng, T. Akasaka and S. Nagase, *Chem. Soc. Rev.*, 2012, **41**, 7723–7760.
- 6 D. M. Rivera-Nazario, J. R. Pinzón, S. Stevenson and L. A. Echegoyen, *J. Phys. Org. Chem.*, 2013, **26**, 194–205.
- 7 J.-Y. Zhang, Y.-Q. Ye, Y. Chen, C. Pregot, T.-H. Li, S. Balasubramaniam, D. B. Hobart, Y.-F. Zhang, S. Wi, R. M. Davis, L. A. Madsen, J. R. Morris, S. M. LaConte, G. T. Yee and H. C. Dorn, *J. Am. Chem. Soc.*, 2014, **136**, 2630–2636.
- 8 J.-F. Zhang, P. P. Fatouros, C.-Y. Shu, J. Reid, L. S. Owens, T. Cai, H. W. Gibson, G. L. Long, F. D. Corwin, Z.-J. Chen and H. C. Dorn, *Bioconjugate Chem.*, 2010, **21**, 610–615.
- 9 M. Yamada, H. Kurihara, M. Suzuki, J.-D. Guo, M. Waelchli, M. M. Olmstead, A. L. Balch, S. Nagase, Y. Maeda, T. Hasegawa, X. Lu and T. Akasaka, *J. Am. Chem. Soc.*, 2014, **136**, 7611–7614.
- 10 T. Wakahara, H. Nikawa, T. Kikuchi, T. Nakahodo, G. M. A. Rahman, T. Tsuchiya, Y. Maeda, T. Akasaka, K. Yoza, E. Horn, K. Yamamoto, N. Mizorogi, Z. Slanina and S. Nagase, *J. Am. Chem. Soc.*, 2006, **128**, 14228–14229.
- 11 M. Suzuki, N. Mizorogi, T. Yang, F. Uhlík, Z. Slanina, X. Zhao, M. Yamada, Y. Maeda, T. Hasegawa, S. Nagase, X. Lu and T. Akasaka, *Chem.–Eur. J.*, 2013, **19**, 17125–17130.
- 12 X. Lu, T. Akasaka and S. Nagase, *Chem. Commun.*, 2011, **47**, 5942–5957.

- 13 A. A. Popov, S.-F. Yang and L. Dunsch, *Chem. Rev.*, 2013, **113**, 5989–6113.
- 14 A. A. Popov and L. Dunsch, *J. Am. Chem. Soc.*, 2007, **129**, 11835–11849.
- 15 A. A. Popov and L. Dunsch, *Chem.–Eur. J.*, 2009, **15**, 9707–9729.
- 16 A. Rodríguez-Forteza, N. Alegret, A. L. Balch and J. M. Poblet, *Nat. Chem.*, 2010, **2**, 955–961.
- 17 M. García-Borràs, S. Osuna, J. M. Luis, M. Swart and M. Solà, *Chem. Soc. Rev.*, 2014, **43**, 5089–5105.
- 18 N. Tagmatarchis, E. Aslanis, K. Prassides and H. Shinohara, *Chem. Mater.*, 2001, **13**, 2374–2379.
- 19 S.-F. Yang and L. Dunsch, *Angew. Chem., Int. Ed.*, 2006, **45**, 1299–1302.
- 20 Y.-F. Lian, Z.-J. Shi, X.-H. Zhou and Z.-N. Gu, *Chem. Mater.*, 2004, **16**, 1704–1714.
- 21 A. A. Popov, L. Zhang and L. Dunsch, *ACS Nano*, 2010, **4**, 795–802.
- 22 W. Xu, L. Feng, M. Calvaresi, J. Liu, Y. Liu, B. Niu, Z.-J. Shi, Y.-F. Lian and F. Zerbetto, *J. Am. Chem. Soc.*, 2013, **135**, 4187–4190.
- 23 Z.-D. Xu, T. Nakane and H. Shinohara, *J. Am. Chem. Soc.*, 1996, **118**, 11309–11310.
- 24 T. Pichler, M. Knupfer, M. S. Golden, T. Böske, J. Fink, U. Kirbach, P. Kuran, L. Dunsch and C. Jung, *Appl. Phys. A: Mater. Sci. Process.*, 1998, **66**, 281–285.
- 25 S. Nagase and K. Kobayashi, *Chem. Phys. Lett.*, 1993, **214**, 57–63.
- 26 K. Suenaga, S. Iijima, H. Kato and H. Shinohara, *Phys. Rev. B: Condens. Matter Mater. Phys.*, 2000, **62**, 1627–1630.
- 27 H. Yamaoka, H. Sugiyama, Y. Kubozono, A. Kotani, R. Nouchi, A. M. Vlaicu, H. Oohashi, T. Tochio, Y. Ito and H. Yoshikawa, *Phys. Rev. B: Condens. Matter Mater. Phys.*, 2009, **80**, 205403.
- 28 H. W. Kroto, J. R. Heath, S. C. O'Brien, R. F. Curl and R. E. Smalley, *Nature*, 1985, **318**, 162–163.
- 29 J. Janaki, G. V. N. Rao, V. S. Sastry, Y. Hariharan, T. S. Radhakrishnan, C. S. Sundar, A. Bharati, M. C. Valsakumar and N. Subramanian, *Solid State Commun.*, 1995, **94**, 37–40.
- 30 L. Epple, K. Y. Amsharov and M. Jansen, *Fullerenes, Nanotubes, Carbon Nanostruct.*, 2009, **17**, 67–77.
- 31 F. H. Hennrich, R. H. Michel, A. Fischer, S. Richard-Schneider, S. Gilb, M. M. Kappes, D. Fuchs, M. Bürk, K. Kobayashi and S. Nagase, *Angew. Chem., Int. Ed.*, 1996, **35**, 1732–1734.
- 32 C.-R. Wang, T. Sugai, T. Kai, T. Tomiyama and H. Shinohara, *Chem. Commun.*, 2000, 557–558.
- 33 T. S. M. Wan, H.-W. Zhang, T. Nakane, Z.-D. Xu, M. Inakuma, H. Shinohara, K. Kobayashi and S. Nagase, *J. Am. Chem. Soc.*, 1998, **120**, 6806–6807.
- 34 P. W. Fowler and D. E. Manolopoulos, *An Atlas of Fullerenes*, Clarendon Press, Oxford, 1995, pp. 15–42.
- 35 Z. Slanina, K. Ishimura, K. Kobayashi and S. Nagase, *Chem. Phys. Lett.*, 2004, **384**, 114–118.
- 36 K. Ziegler, A. Mueller, K. Y. Amsharov and M. Jansen, *J. Am. Chem. Soc.*, 2010, **132**, 17099–17101.
- 37 K. Raghavachari, *Z. Phys. D: At., Mol. Clusters*, 1993, **26**, S261–S263.
- 38 K. Bucher, L. Epple, J. Mende, M. Mehring and M. Jansen, *Phys. Status Solidi B*, 2006, **243**, 3025–3027.
- 39 Z.-Y. Wang, Y. Nakanishi, S. Noda, H. Niwa, J.-Y. Zhang, R. Kitaura and H. Shinohara, *Angew. Chem., Int. Ed.*, 2013, **52**, 11770–11774.
- 40 X. Lu, H. Nikawa, T. Tsuchiya, Y. Maeda, M. O. Ishitsuka, T. Akasaka, M. Toki, H. Sawa, Z. Slanina, N. Mizorogi and S. Nagase, *Angew. Chem., Int. Ed.*, 2008, **47**, 8642–8645.
- 41 M. Yamada, T. Wakahara, T. Tsuchiya, Y. Maeda, T. Akasaka, N. Mizorogi and S. Nagase, *J. Phys. Chem. A*, 2008, **112**, 7627–7631.
- 42 N. Chen, C. M. Beavers, M. Mulet-Gas, A. Rodríguez-Forteza, E. J. Munoz, Y. Y. Li, M. M. Olmstead, A. L. Balch, J. M. Poblet and L. Echegoyen, *J. Am. Chem. Soc.*, 2012, **134**, 7851–7860.
- 43 K. Bucher, J. Mende, M. Mehring and M. Jansen, *Fullerenes, Nanotubes, Carbon Nanostruct.*, 2007, **15**, 29–42.
- 44 K. Akiyama, T. Hamano, Y. Nakanishi, E. Takeuchi, S. Noda, Z.-Y. Wang, S. Kubuki and H. Shinohara, *J. Am. Chem. Soc.*, 2012, **134**, 9762–9767.
- 45 T. Ogawa, T. Sugai and H. Shinohara, *J. Am. Chem. Soc.*, 2000, **122**, 3538–3539.
- 46 M. Ishibashi, Y. Tomioka and Y. Taniguchi, *Jpn. J. Appl. Phys.*, 1994, **33**, L258–L259.
- 47 J.-Q. Ding and S.-F. Yang, *J. Am. Chem. Soc.*, 1996, **118**, 11254–11257.
- 48 Q. Zhou, H. Li, Y.-F. Lian, M. Suzuki, L.-P. Bao, W.-T. Cai, W.-W. Wang, S. Nagase, X. Lu and T. Akasaka, *Chem. Commun.*, 2014, **50**, 9876–9878.
- 49 A. D. Becke, *Phys. Rev. A: At., Mol., Opt. Phys.*, 1988, **38**, 3098–3100.
- 50 C. Lee, W.-T. Yang and R. G. Parr, *Phys. Rev. B: Condens. Matter Mater. Phys.*, 1988, **37**, 785–789.
- 51 M. S. Gordon, J. S. Binkley, J. A. Pople, W. J. Pietro and W. J. Hehre, *J. Am. Chem. Soc.*, 1982, **104**, 2797–2803.
- 52 W. J. Hehre, R. Ditchfield and J. A. Pople, *J. Chem. Phys.*, 1972, **56**, 2257–2261.
- 53 M. Dolg, H. Stoll and H. Preuss, *Theor. Chim. Acta*, 1993, **85**, 441–450.
- 54 P. J. Hay and W. R. Wadt, *J. Chem. Phys.*, 1985, **82**, 299–310.
- 55 Y. Zhao and D. G. Truhlar, *Theor. Chem. Acc.*, 2008, **120**, 215–241.
- 56 T. R. Cundari and W. J. Stevens, *J. Chem. Phys.*, 1993, **98**, 5555–5565.
- 57 M. Dolg, H. Stoll, A. Savin and H. Preuss, *Theor. Chim. Acta*, 1989, **75**, 173–194.
- 58 A. E. Reed, R. B. Weinstock and F. Weinhold, *J. Chem. Phys.*, 1985, **83**, 735–746.
- 59 R. C. Haddon, *Science*, 1993, **261**, 1545–1550.
- 60 R. C. Haddon, *J. Phys. Chem. A*, 2001, **105**, 4164–4165.
- 61 Z. Slanina, *Int. Rev. Phys. Chem.*, 1987, **6**, 251–267.
- 62 H. Shinohara, *Rep. Prog. Phys.*, 2000, **63**, 843–892.
- 63 T. Kodama, R. Fujii, Y. Miyake, S. Suzuki, H. Nishikawa, I. Ikemoto, K. Kikuchi and Y. Achiba, *Chem. Phys. Lett.*, 2004, **399**, 94–97.
- 64 W. Xu, B. Niu, Z.-J. Shi, Y.-F. Lian and L. Feng, *Nanoscale*, 2012, **4**, 6876–6879.

- 65 F.-F. Li, N. Chen, M. Mulet-Gas, V. Triana, J. Murillo, A. Rodríguez-Forteza, J. M. Poblet and L. Echegoyen, *Chem. Sci.*, 2013, **4**, 3404–3410.
- 66 T. Akasaka, X. Lu, H. Kuga, H. Nikawa, N. Mizorogi, Z. Slanina, T. Tsuchiya, K. Yoza and S. Nagase, *Angew. Chem., Int. Ed.*, 2010, **49**, 9715–9719.
- 67 Y. Maeda, M. Kimura, C. Ueda, M. Yamada, T. Kikuchi, M. Suzuki, W.-W. Wang, N. Mizorogi, N. Karousis, N. Tagmatarchis, T. Hasegawa, M. M. Olmstead, A. L. Balch, S. Nagase and T. Akasaka, *Chem. Commun.*, 2014, **50**, 12552–12555.
- 68 H. Nikawa, T. Yamada, B. P. Cao, N. Mizorogi, Z. Slanina, T. Tsuchiya, T. Akasaka, K. Yoza and S. Nagase, *J. Am. Chem. Soc.*, 2009, **131**, 10950–10954.
- 69 Y. Takano, M. O. Ishitsuka, T. Tsuchiya, T. Akasaka, T. Kato and S. Nagase, *Chem. Commun.*, 2010, **46**, 8035–8036.
- 70 S. Sato, Y. Maeda, J.-D. Guo, M. Yamada, N. Mizorogi, S. Nagase and T. Akasaka, *J. Am. Chem. Soc.*, 2013, **135**, 5582–5587.
- 71 Z. Slanina, F. Uhlík, S.-L. Lee, L. Adamowicz, H. Kurihara, H. Nikawa, X. Lu, M. Yamada, S. Nagase and T. Akasaka, *Fullerenes, Nanotubes, Carbon Nanostruct.*, 2014, **22**, 173–181.
- 72 T. Yang and X. Zhao, *Chem. Phys.*, 2013, **423**, 173–177.
- 73 C. Tang, W. Zhu and K. Deng, *J. Mol. Struct.: THEOCHEM*, 2009, **894**, 112–116.
- 74 X.-G. Liu, M. Chi, P.-D. Han, Z.-X. Zhang, X.-H. Fang, W. Jia and B.-S. Xu, *J. Mol. Struct.: THEOCHEM*, 2007, **818**, 71–75.
- 75 Z. Slanina, F. Uhlík, S.-L. Lee, L. Adamowicz, T. Akasaka and S. Nagase, *Molecules*, 2012, **17**, 13146–13156.
- 76 S. Nagase, K. Kobayashi and T. Akasaka, *J. Mol. Struct.: THEOCHEM*, 1999, **461–462**, 97–104.
- 77 Z. Slanina, K. Kobayashi and S. Nagase, *Chem. Phys. Lett.*, 2003, **372**, 810–814.
- 78 M. Chi, Z.-X. Zhang, P.-D. Han, X.-H. Fang, W. Jia, H.-B. Dong and B.-S. Xu, *J. Mol. Model.*, 2008, **14**, 465–470.
- 79 X. Lu, H. Nikawa, T. Kikuchi, N. Mizorogi, Z. Slanina, T. Tsuchiya, S. Nagase and T. Akasaka, *Angew. Chem., Int. Ed.*, 2011, **50**, 6356–6359.
- 80 J. H. Weaver, Y. Chai, G. H. Kroll, C. Jin, T. R. Ohno, R. E. Hauffer, T. Guo, J. M. Alford, J. Conceicao, L. P. F. Chibante, A. Jain, G. Palmer and R. E. Smalley, *Chem. Phys. Lett.*, 1992, **190**, 460–464.
- 81 H.-X. Jin, H. Yang, M.-L. Yu, Z.-Y. Liu, C. M. Beavers, M. M. Olmstead and A. L. Balch, *J. Am. Chem. Soc.*, 2012, **134**, 10933–10941.